FULL LENGTH	Iranian Biomedical Journal 29 (3): 114-125 May 2025

Atorvastatin-Loaded Carboxymethyl Cellulose-Gelatin Hydrogel: A Synergistic Strategy for Enhanced Wound Healing and Skin Tissue Regeneration

Seyed Reza Mousavi[1], Mojtaba Rashidi[2], Azam Khedri[1], Maryam Kouchak[3], Majid Salehi[4≠], Sepehr Zamani[5], Ghorban Mohammadzadeh[2*]

[1]Department of Clinical Biochemistry, School of Medicine, Ahvaz Jundishapur University of Medical Sciences, Ahvaz, Iran; [2]Hyperlipidemia Research Center, Department of Clinical Biochemistry, School of Medicine, Ahvaz Jundishapur University of Medical Sciences, Ahvaz, Iran; [3]Department of Pharmaceutics, Faculty of Pharmacy, Nanotechnology Research Center, Ahvaz Jundishapur University of Medical Sciences, Ahvaz, Iran; [4]Regenerative Medicine Research Center, Shahroud University of Medical Sciences, Shahroud, Iran; [5]Department of Tissue Engineering, School of Medicine, Shahroud University of Medical Sciences, Shahroud, Iran

OPEN ACCESS

Article type: Research Article
Received: April 19, 2025
Revised: May 17, 2025
Accepted: May 27 2025
Published online: May 28, 2025

How to cite:
Mousavi SR, Rashidi M, Khedri A, Kouchak M, Salehi M, Zamani S, Mohammadzadeh G. Atorvastatin-Loaded Carboxymethyl Cellulose-Gelatin Hydrogel: A Synergistic Strategy for Enhanced Wound Healing and Skin Tissue Regeneration. *Iran. Biomed. J.* 2025; 29(3): 114-125.

This article is licensed under a Creative Commons Attribution-NonDerivatives 4.0 International License.

ABSTRACT

Background: Skin tissue engineering is an innovative alternative to traditional methods for addressing skin injuries. This study aimed to synthesize a hydrogel consisting of CMC and Gel containing ATR with the potential to accelerate tissue regeneration and wound healing in an animal model.

Methods: Five unique formulations of hydrogel with different concentrations of ATR (0.1%, 0.5%, 1%, and 2% w/v) were synthesized using CMC-Gel. The structural characteristics of the hydrogels were assessed using SEM and FTIR spectroscopy. Additional evaluations carried out included swelling behavior, degradability, ATR release, compatibility, hemolytic activity, and the viability of NIH/3T3 fibroblast cells. The therapeutic effectiveness of these hydrogels in enhancing wound healing was investigated in an animal model by making a full-thickness skin incision in Wistar rats.

Results: The synthesized CMC-Gel scaffolds had a porous structure with interconnected pores measuring 103 ± 8.74 µm and the ability to enhance cell migration. The MTT analysis showed a concentration-dependent relationship between ATR and cell proliferation, among which, the desirable concentration was 0.1% w/v. Furthermore, increased ATR concentrations were associated with decreased dressing capacity for hemostasis and coagulation. In vivo studies revealed that all the hydrogel-treated groups significantly outperformed the control group in promoting wound closure rates. Remarkably, the CMC-Gel-ATR 0.1% group exhibited the highest rates of wound closure, re-epithelialization, and angiogenesis.

Conclusion: Our results suggest the CMC-Gel-ATR as a desirable wound dressing for clinical application due to its unique physicochemical properties and comprehensive biocompatibility in in vitro and in vivo investigations.
DOI: 10.61882/ibj.5031

Keywords: Angiogenesis, Atorvastatin, Biopolymers

Corresponding Author: Ghorban Mohammadzadeh
Hyperlipidemia Research Center, Department of Clinical Biochemistry, School of Medicine, Ahvaz Jundishapur University of Medical Sciences, Ahvaz, Iran; Tel.: (+98-911) 13436812; E-mail: mohammadzadeh@ajums.ac.ir; ORCID ID: 0000-0001-7921-4770

#Co-corresponding author

List of Abbreviations:
ATR: atorvastatin; **BCI:** blood clotting index; **CMC:** carboxymethyl cellulose; **FBS:** fetal bovine serum; **FTIR:** fourier-transform infrared spectroscopy; **Gel:** gelatin; **H & E:** hematoxylin and eosin; **MTT:** 3'-(4,5-Dimethylthiazol-2-yl)-2,5-diphenyl tetrazolium bromide; **PBS:** phosphate-buffered saline; **SEM:** scanning electron microscopy

[Downloaded from ibj1.pasteur.ac.ir on 2026-10-17]
[DOI: 10.61882/ibj.5043]

INTRODUCTION

Skin injuries are among the most common medical issues, often resulting in high medical costs, reduced individual productivity, and limited physical activities[1]. These injuries disrupt the normal function of the skin, causing the body to lose essential fluids and proteins, alter metabolic processes, and affect the circulatory and defense systems[2].

Traditionally, wound treatment strategies included natural substances such as honey and plant extracts. Today, numerous types of dressings have been developed to accelerate wound healing. One of the most significant advancements in dressing production is the use of polymeric materials. Among them, hydrogels have a special capability because of their three-dimensional network structure. Additionally, due to their fluid-absorption capacity, these materials can efficiently absorb exudate from wounds and make a moist wound environment[3].

CMC and Gel are two natural and semi-synthetic polymers that are used to create biomedical hydrogels. CMC features with attractive surface characteristics enhance protein adsorption, facilitate cell aggregation and differentiation, and provide low degradation rates, high mechanical strength, along with excellent biocompatibility. Furthermore, CMC can retain moisture in wound areas, which promotes the growth of the extracellular matrix and regeneration of the epithelium[4]. Gel, another biocompatible polymer produced by hydrolyzing collagen, provides several advantages, including biosafety, compatibility with biological systems, non-toxicity, and cost-effectiveness. Its amino acid sequences, such as RGD, enhance hemostasis and stimulate cell adhesion and proliferation throughout the healing process[5].

ATR is a member of the second generation of statins. In addition to the anti-inflammatory properties, statins are a viable option for wound healing as they can control cellular processes[6]. Studies have explored the effectiveness of statins in treating wounds and skin disorders by using different formulations and administration methods, including intraperitoneal injection and oral intake. However, like other systemic medications, oral statins have side effects such as myopathy and liver problems[7]. Topical drug delivery approaches are suggested as a feasible substitute for oral statins in the wound healing process. This approach can minimize side effects, improve therapeutic effects, and enhance medication delivery[8].

The present study aimed to exhibit that the incorporation of ATR into a CMC-Gel hydrogel could enhance wound healing by modulating the wound microenvironment and improving tissue regeneration. While the therapeutic potential of ATR has been well established, its integration into biopolymer-based topical scaffolds has remained underexplored. We hypothesize that embedding ATR in a CMC-Gel scaffold can promote wound healing by enhancing moisture retention, supporting cell viability and proliferation, and facilitating tissue regeneration. This approach addresses the limitations of conventional treatments and contributes to the development of multifunctional and bioactive wound care systems. To our knowledge, the combination of CMC, Gel, and ATR in a topical hydrogel formulation has not been extensively investigated, representing a novel advancement in hydrogel-based wound healing approaches.

MATERIALS AND METHODS

Materials

MTT, CMC, and Gel powder (bovine skin, type B) were purchased from Sigma-Aldrich (USA). Trypsin-EDTA, DMEM, FBS, and penicillin-streptomycin were supplied by Gibco (Germany). ATR was obtained from Daana Pharmaceutical Company (Tabriz, Iran). The Pasteur Institute of Iran in Tehran provided the fibroblast cell line NIH/3T3.

Synthesis of CMC-Gel and CMC-Gel-ATR Hydrogels

CMC powder (4% w/v) and Gel powder (3% w/v) were dissolved in deionized water (8:1) under stirring at 400 rpm for 12 hours at room temperature. ATR was then added to the mixture and homogenized for six hours. Afterwards, phenoxyethanol was added to 0.9% of the final volume of the hydrogel to enhance stability and provide antiseptic properties (Table 1). The hydrogels were preserved at -80 °C for 16 hours and then transferred to a freeze dryer (Terrace, Spain), set at -54 °C for 48 hours, which allowed a porous structure to be formed[9].

Characterization of the scaffolds

Scanning electron microscopy

SEM was used to evaluate the surface properties of the generated lyophilized hydrogels (SEM; DSM 960A, Zeiss, Germany). To improve conductivity, a small layer of gold was applied to the freeze-dried hydrogels (SCD 004, Balzers, Germany). Image J and Origin Pro software were used to determine the average pore diameter. For this assessment, 20 randomly chosen places within each image were scanned[10].

[Downloaded from ibj1.pasteur.ac.ir on 2026-10-17]

[DOI: 10.61882/ibj.5043]

Table 1. CMC-Gel-ATR formulation for preparing 1 mL of hydrogel

Hydrogel (sample)	CMC:Gel (% v/v)	Polymer (% w/v)	ATR concentration (mg/ml)	Phenoxyethanol (% v/v)
CMC-Gel	8:1	4:3	0	0.9
CMC-Gel-ATR 1 (0.1% w/v)	8:1	4:3	1	0.9
CMC-Gel-ATR 5 (0.5% w/v)	8:1	4:3	5	0.9
CMC-Gel-ATR 10 (1% w/v)	8:1	4:3	10	0.9
CMC-Gel-ATR 20 (2% w/v)	8:1	4:3	20	0.9

Fourier-transform infrared spectroscopy

FTIR was utilized to examine the interactions among functional groups in different hydrogel structures, particularly CMC-Gel and CMC-Gel-ATR. The FTIR spectroscopy technique (Spectrum GX, PerkinElmer, USA) was used to record the FTIR spectra spanning a wavelength range of 400 to 4000 cm^{-1}[11].

Hydrogel assessments

Degradation

The rate of degradation was assessed by measuring the weight loss of the hydrogel samples. Before submerging the dried hydrogels in PBS solution (pH 7.4), we recorded their weights (W_0). The samples were then immersed in the PBS solution for the predetermined intervals of 2, 6, 12, 24, and 48 hours. After each interval, excess solution was removed from the samples before reweighing them (W_1). The percentage of weight reduction was finally calculated using the formula given in Equation (1)[12].

$$\text{Weight loss (\%)} = \frac{\text{W0} - \text{W1}}{\text{W0}} \times 100 \quad (1)$$

Water uptake

The ability of hydrogel samples to absorb water was evaluated at room temperature. Freeze-drying procedure was used to lyophilize the hydrogels. The initial weights of the freeze-dried samples (W_0) were recorded before their immersion in PBS for varying periods (3, 6, 12, 18, 24, and 48 hours). The samples were reweighed (W_1) at each specified time interval, and equation (2) was used to determine the water absorption[13].

$$\text{Water absorption (\%)} = \frac{\text{W1} - \text{W0}}{\text{W0}} \times 100 \quad (2)$$

Blood compatibility

Rat blood (2 mL) was diluted with 2.5 mL of normal saline. The diluted blood sample (200 µL) was then added to three identical hydrogel samples (100 µL) prepared in 96-well plates. After 1 hour of incubation at 37 °C, the plates were centrifuged (377 ×g, 10 minutes). A negative control was prepared by combining 4 mL of normal saline with 200 µL of diluted blood, while a positive control was prepared by mixing 4 mL of distilled H_2O with 200 µL of diluted blood[14]. The supernatant was then tested for absorbance at 545 nm, and the percentage of hemolysis was determined using Equation (3).

$$\text{Hemolysis (\%)} = \frac{\text{Ds} - \text{Dnc}}{\text{Dpc} - \text{Dnc}} \times 100 \quad (3)$$

Blood clotting index

Fresh rat blood was diluted in a citrated tube to measure the blood coagulation index of the samples. Next, 1.5 mL of each sample was incubated at 37 °C for 1 hour. The samples were then combined with 100 µL of blood from rats. The mixture was incubated (5 minutes) before adding 0.2 M of $CaCl_2$. After an additional five minutes, each sample was mixed with 25 mL of distilled H_2O. The resultant suspensions were transferred to a 96-well plate for further analysis following a final incubation of five minutes. To create the control samples, we combined 25 mL of deionized H_2O with 100 µL of fresh human blood[15]. Using equation (4), we measured the relative absorbance of the hydrogel samples at 545 nm to calculate the BCI.

$$\text{BCI (\%)} = \frac{\text{A sample}}{\text{A control}} \times 100 \quad (4)$$

Cytotoxicity test

The effect of CMC/Gel and CMC/Gel/ATR hydrogel dressing extracts on NIH/3T3 fibroblast cell line was carried out by using the MTT assay. The NIH/3T3 fibroblast cell line was seeded at a density of 1×10^4 cells per well in a sterile 96-well plate containing DMEM supplemented with 10% FBS. The cells were then incubated with 5% CO_2 at 37 °C overnight. To prepare hydrogel extracts, we incubated hydrogel samples containing different concentrations of ATR with DMEM for 48 hours under sterile conditions. After a 24-hour incubation period, 100 µL of the extracts was added to each well in triplicate. Following the incubation period, 20 µL of MTT solution (5 mg/mL) was added to each well, and the supernatants were discarded. After an additional three hours of incubation, 100 µL of DMSO was added to dissolve the formazan

[Downloaded from ibj1.pasteur.ac.ir on 2026-10-17]

[DOI: 10.61882/ibj.5043]

crystals[16]. The absorbance at 570 nm was then measured using a plate reader to determine the percentage of cell viability, which was calculated using equation 5.

$$\text{Cell viability (\%)} = \frac{\text{absorbance of sample}}{\text{absorbance of control}} \times 100 \quad (5)$$

Release of ATR

To determine the amount of ATR released from the CMC-Gel hydrogel, a standard curve was created for ATR using a concentration range of 0.1 to 100 mg/mL. CMC-Gel-ATR hydrogel (1 mg/mL) was placed in 5 mL of the simulated body fluid in a shaker incubator at 37 °C with a speed of 50 rpm. The absorbance of the supernatants was measured at 246 nm at different time intervals (2, 4, 6, 12, 24, 36, 48, 72, and 96 hours) to evaluate the ATR release[17]. Finally, by using the established standard curve, we obtained the quantitative values.

pH measurements

At the predetermined intervals of 2, 4, 6, 12, 24, and 48 hours, the pH of the normal saline containing the hydrogel samples was measured at room temperature using a digital pH meter (pH/mV Meter, 86502 AZ) to monitor any potential pH variations induced by the hydrogel[18].

In vivo test

Adult male Wistar rats (n = 18, weighing 200–250 g) were purchased from Shahroud University of Medical Sciences (Shahroud, Iran). The animals were provided food and water in the standard housing conditions. The produced hydrogels were evaluated for their effectiveness in wound healing using a full-thickness wound model (1.5 × 1.5 cm^2). Rats were intraperitoneally injected with 100 mg/kg of ketamine and 10 mg/kg of xylazine to induce anesthesia. The dorsal skin of rats was cleaned, shaved, and disinfected using 70% alcohol. Afterwards, the rats were randomly divided into three groups of six. Group 1: negative control (treated with sterile gauze); group 2: rats treated with CMC-Gel hydrogel; group 3: rats treated with CMC-Gel-ATR hydrogel. The animals were sacrificed 14 days after the procedure, and the wound tissue was collected for histological analysis. Photographs taken 14 days following surgery were used to monitor the wound healing process[19]. Image J software was used to evaluate the results. Equation 6 was employed to calculate the percentages of wound closure.

$$\text{Wound closure (\%)} = 1 - \frac{\text{wound area}}{\text{initial area}} \times 100 \quad (6)$$

Histopathological analysis

The development of granulation tissue, angiogenesis, scar formation, collagen deposition, and re-epithelialization was assessed using Masson's trichrome and H&E stainings. Tissue specimens were preserved in 10% formalin for histological examination. After being dehydrated and fixed in paraffin, the specimens were cut into 5 µm-thick sections[20]. We used a light microscope (Olympus BX51; Olympus, Tokyo, Japan) to analyze the histology slides.

Statistical analysis

GraphPad Prism 10.2.2 software was used for all statistical analyses. For normally distributed data, a one-way analysis of variance (ANOVA), followed by Tukey's post hoc test, was used for multiple group comparisons. For non-normally distributed data, we applied the Kruskal–Wallis test, followed by the Mann–Whitney U test. Data are presented as mean ± SD. A p value < 0.05 was considered statistically significant.

RESULTS

Morphological properties of hydrogels

The SEM analysis of the CMC-Gel scaffold (Fig. 1A-1C) revealed a porous architecture characterized by large pores (103 ± 8.74 µm), which may not be ideal for promoting cell adhesion and migration. In contrast, the CMC-Gel-ATR20 scaffold (Fig. 1D-1F) exhibited a fine porosity and a more consistent fibrous network (62.39 ± 5.07), offering an increased surface area for cell attachment. Recent research indicates that this characteristic is crucial for enhancing the regeneration of damaged tissues. Therefore, incorporating ATR into the CMC-Gel-ATR scaffold has improved its functional attributes[21].

FTIR spectra characteristics

Figure 1G and 1H show the results of FTIR spectra of CMC-Gel and CMC-Gel-ATR20 scaffolds. A broad band at 3400–3300 cm^{-1} corresponds to O–H and N–H stretching in CMC and Gel, respectively. The peak near 2900 cm^{-1} associates with CMC and amide I from Gel, while 1550 cm^{-1} corresponds to the amide II bond. The peak at 1420 cm^{-1} reflects symmetric COO^- stretching, and the peaks in the range between 1050 and 1100 cm^{-1} relate to C–O–C and C–O stretching. Shifts in these bands suggest hydrogen bonding between CMC and Gel, confirming their compatibility (Fig. 1G). For CMC-Gel-ATR20 (Fig. 1H), the peaks at 1695.04 and 1714.72 cm^{-1} indicate C=O stretching associated with ATR.

[Downloaded from ibj1.pasteur.ac.ir on 2026-10-17]

[DOI: 10.61882/ibj.5043]

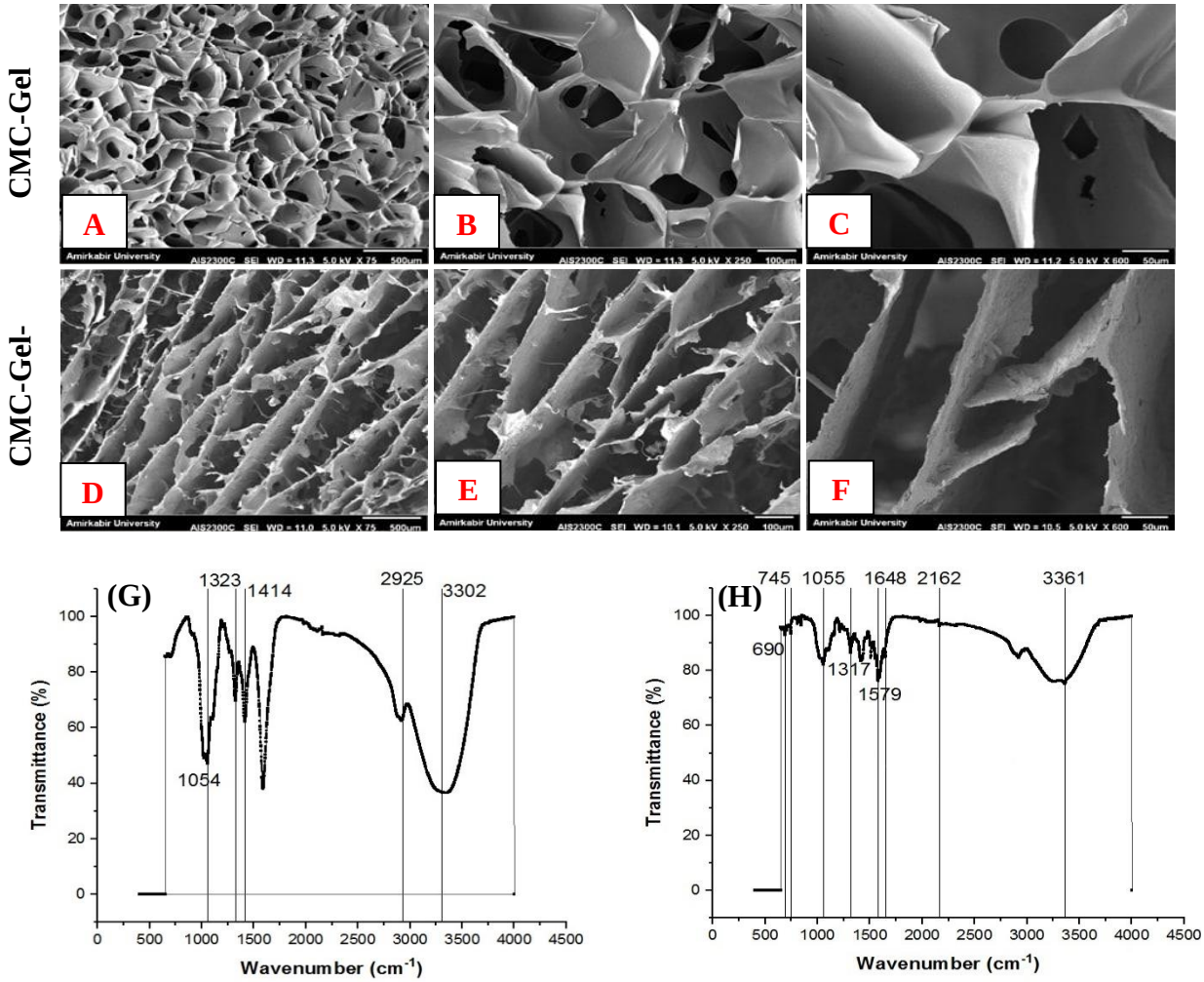

Fig 1. SEM images of CMC-Gel (A, B, C) and , CMC-Gel-ATR (D, E, F) with 75×, 250×, and 500× magnifications. FTIR spectrums of CMC-Gel (G) and CMC-Gel-ATR20 (H).

Additional peaks at 1648.21 and 2162.04 cm^{-1} likely correspond to the conjugated C=C vibrations in aromatic rings. Bands at 1579.07, 1591.27, and 1517.63 cm^{-1} further support the presence of aromatic structures. The 1404 to 1424 cm^{-1} region relates to the C–H bending or ester C–O stretching, and the 689.96 cm^{-1} band confirms the presence of mono-substituted benzene rings. These findings affirm the successful incorporation of ATR.

Degradation behavior of hydrogels

The weight loss of the scaffolds was assessed at intervals of 2, 6, 12, 24, and 48 hours. CMC-Gel showed the highest degradation (98.08 ± 3.21%) at 48 h, followed by CMC-Gel-ATR1 (94.5 ± 5.36%), ATR5 (93.5 ± 2.12%), ATR20 (88.5 ± 2.13%), and ATR10 (87 ± 4.24%). After 2 hours, the degradation rates were as follows: 22 ± 2.82% (CMC-Gel), 19 ± 1.41% (CMC-Gel-ATR1), 13.5 ± 2.12% (ATR5), 19.5 ± 0.78% (ATR20), and 12.5 ± 0.79% (ATR10). Although the water insolubility of ATR may influence scaffold degradation at higher concentrations, no statistically significant differences were observed among the treatment groups at any time point ($p > 0.05$). All comparisons were made relative to the CMC-Gel group.

Swelling behavior of hydrogels

All groups demonstrated a time-dependent increase in water uptake from 3 to 48 hours. CMC-Gel exhibited the highest swelling rates, reaching 16.5 ± 2.12%, 85.22 ± 10.21%, and 109.01 ± 12.94% at 3, 24, and 48 hours, respectively. Although ATR-containing hydrogels showed a similar swelling trend over time, a concentration-dependent reduction in water absorption was observed. After 48 hours of incubation in PBS solution, the percentage of water uptake of hydrogels

[Downloaded from ibj1.pasteur.ac.ir on 2026-10-17]
[DOI: 10.61882/ibj.5043]

with different concentration of ATR (1, 5, 10, and 20 mg/mL) was 108 ± 10.53%, 96.5 ± 7.26%, 94 ± 6.05%, and 77.5 ± 3.92%, respectively. Notably, the ATR20 showed a significant reduction in water uptake compared to CMC-Gel at both 24 and 48 hours (67 ± 2.82% vs. 85.22 ± 10.21%) ($p < 0.05$), while other groups did not exhibit any significant difference.

Hemolysis behavior of hydrogels

The hemolysis rate in the CMC-Gel was 4.71 ± 1.39%. The ATR-containing groups showed a concentration-dependent hemolysis rate as follows: ATR1 (2.5 ± 1.3%), ATR5 (3.57 ± 1.35%), ATR10 (3.81 ± 1.25%), and ATR20 (5.47 ± 1.49%). All treatment groups differed significantly from the negative control group with a hemolysis rate of 0.2 ± 0.1% ($p < 0.05$). In contrast, the positive control showed a highly significant increase in the hemolysis rate, 99.33 ± 5.37% ($p < 0.0001$). An increase in the ATR concentration resulted in enhanced hemolysis, implying that only ATR20 exhibited potential hemolytic effects.

BCI of hydrogels

The BCI value of the CMC-Gel scaffold was found to be 27.31 ± 4.15%. A concentration-dependent increase was observed in BCI. The BCI values for CMC-Gel-ATR1, ATR5, and ATR10 were 29.06 ± 3.3%, 33.57 ± 3.84%, and 37.84 ± 4.25%, respectively, with no statistically significant differences compared to CMC-Gel ($p > 0.05$). However, the CMC-Gel-ATR20 demonstrated a significant increase in BCI (44.39 ± 6.70%; $p < 0.01$), indicating reduced clotting potential at higher ATR concentrations. The positive control showed a BCI value of 100.33 ± 5.39%, which was highly significantly different from the CMC-Gel ($p < 0.0001$). This outcome suggests the effectiveness of ATR as a wound dressing, which is highly dependent on concentration, i.e. at high concentrations, it may not be effective for managing bleeding wounds.

Cell cytotoxicity results

The cytotoxic effects of the prepared hydrogels on the fibroblast cells are presented in Figure 2. These results indicate that low concentrations of ATR can maintain and even improve the fibroblast viability, while higher ATR concentrations may impart cytotoxicity. Therefore, 0.1% ATR was chosen for the animal study.

Results of the ATR release

The cumulative release profile of ATR over various time intervals is illustrated in Figure 3. The amount of the released ATR was quantified by constructing a standard release curve. After 12 and 24 hours, the recorded releases of ATR from the hydrogel were 614.91 ± 22.70 and 780.25 ± 25.41 µg, respectively, leading to a total release of 989.61 ± 14.33 µg over a four-day duration. These results suggest a gradual release of ATR from the CMC-Gel hydrogel, reaching a plateau phase after 36 hours (949.61 ± 33.24 µg). Therefore, from 36 hours onwards, no increase was observed in the amount of ATR released from the hydrogel.

Results of hydrogel pH values

Table 2 reports the pH values of the synthesized hydrogels over 48 hours. All groups, except for CMC-Gel (7.13 ± 0.40), had an acidic pH range (6.22–6.81).

In vivo findings

The study evaluated the efficacy of CMC-Gel and CMC-Gel-ATR1 hydrogels on a full-thickness wound model (Fig. 4A). Wounds of the negative control, which were covered with sterile gauze, exhibited signs of

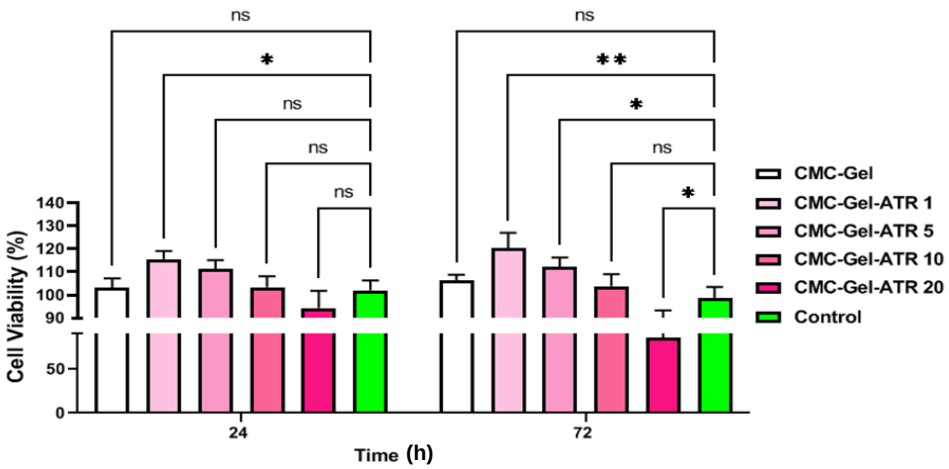

Fig 2. The cytotoxic effects of the prepared hydrogel on the 3T3 fibroblast viability measured by MTT assay at 24 and 72 h. Values represent the mean ± SD; n = 6; ns: not significant; $^{*}p < 0.05$, and $^{**}p < 0.01$.

[Downloaded from ibj1.pasteur.ac.ir on 2026-10-17]

[DOI: 10.61882/ibj.5043]

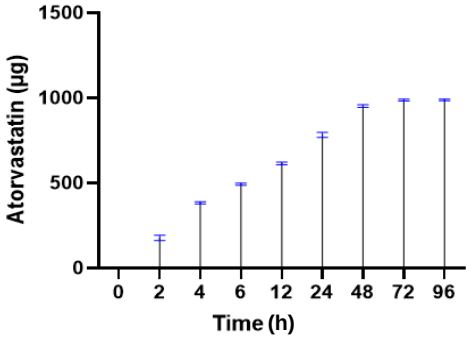

Fig 3. The release of ATR from CMC-gel hydrogel in PBS solution measured after 96 hours in a shaker incubator at 50 rpm at 37 °C. Values represent the mean ± SD (n = 3).

infection and inflammation, and incomplete healing after two weeks. In contrast, the treated groups demonstrated significant healing during the same timeframe. Macroscopic photographic evaluations indicated that one week post-treatment, the hydrogel groups experienced minimal bleeding. Notably, the CMC-Gel-ATR1 yielded the most promising outcomes, showing no indication of infection or inflammation. Figure 4B presents a quantitative analysis of wound healing based on the wound closure rates. The percentages of wound closure on the day seven of treatment in the negative control, CMC-Gel, and CMC-Gel-ATR1 groups were 28.34 ± 10.66%, 39.42 ± 14.39%, and and 52.76 ± 11.91%, respectively. Also, on the day 14 of treatment, the percentages of wound closure in the above group were 70.21 ± 14.28%, 87.66 ± 5.48%, and 93.05 ± 6.17%, respectively. The CMC-Gel-ATR1 showed a significant improvement in wound healing compared to both the control and CMC-Gel groups. Both CMC-Gel and CMC-Gel-ATR1 groups displayed significant improvements compared to the control group on days 7 and 14; however, the effect was more pronounced in the CMC-Gel-ATR1 group ($p < 0.01$ vs. $p < 0.05$). This observation highlights the considerable potential of the CMC-Gel-ATR1 hydrogel in reducing healing time.

Histopathological findings

All treatment groups (negative control, CMC-Gel, and CMC-Gel-ATR1) demonstrated the formation of a distinct epidermal layer after 14 days. The CMC-Gel-ATR1 group showed thicker re-epithelialization and more separation of the dermal layer (Fig. 5L). The CMC-Gel formed a crusty scab, which is a negative aspect of the healing process, as it was absent in the CMC-Gel-ATR1 group Fig. 5H). Blood vessel formation was more pronounced in both the negative control and CMC-Gel-ATR1 groups compared to the CMC-Gel group. However, many blood vessels in the negative control remained immature (Fig. 5C and 5L). Notably, the only CMC-Gel-ATR1 group exhibited the development of skin appendages and resulted in a greater thickness of the dermis layer of the skin (Fig. 5J). The CMC-Gel-ATR1 was particularly successful in forming hair follicles (Fig. 5K). Additionally, an increased number of sebaceous glands was observed (Fig. 5K). Furthermore, collagen fiber synthesis was highest in the CMC-Gel-ATR1 group (Fig. 5K). The findings from Masson's trichrome study of all groups are shown in Figure 6. The formation of collagen fibers in the CMC-Gel-ATR1 group (Fig. 6K) was organized differently compared to the other groups.

DISCUSSION

Wound healing is a dynamic, multi-phase process. It begins with hemostasis, followed by the inflammatory and proliferative phases in order to close the wound. Indeed, during the remodeling phase, collagen fibers are regenerated. Scaffolds made from CMC and Gel are favored for their biocompatibility, mechanical flexibility, and ability to replicate the extracellular matrix[22]. In a previous study, Soleimani et al. demonstrated that a hydrogel composed of CMC gel has satisfying mechanical strength and antibacterial properties. Their study also verified that the hydrogel is non-toxic and plays a significant role in wound healing[23]. Saghafi et al. have demonstrated that topical application of the gel and nanogels containing ATR significantly accelerates wound healing and reduces pain without notable side effects, indicating ATR potential for wound management[8].

Table 2. pH values of hydrogel solutions with and without ATR at different times

Samples	0 h	2 h	4 h	6 h	12 h	24 h	48 h
CMC-Gel	7.18 ± 0.45	7.15 ± 0.39	7.14 ± 0.41	7.15 ± 0.43	7.14 ± 0.38	7.15 ± 0.41	7.13 ± 0.40
CMC-Gel-ATR 1	6.93 ± 0.24	6.84 ± 0.30	6.83 ± 0.28	6.83 ± 0.29	6.82 ± 0.31	6.82 ± 0.29	6.81 ± 0.24
CMC-Gel-ATR 5	6.85 ± 0.25	6.82 ± 0.29	6.82 ± 0.22	6.81 ± 0.26	6.85 ± 0.25	6.82 ± 0.29	6.82 ± 0.22
CMC-Gel-ATR 10	6.72 ± 0.19	6.70 ± 0.22	6.69 ± 0.20	6.68 ± 0.19	6.85 ±0.25	6.82 ± 0.29	6.82 ± 0.22
CMC-Gel-ATR 20	6.35 ± 0.36	6.28 ± 0.25	6.26 ± 0.19	6.25 ± 0.23	6.69 ±0.15	6.67 ± 0.17	6.66 ± 0.16

Values represent the mean ± SD (n = 6).

[Downloaded from ibj1.pasteur.ac.ir on 2026-10-17]

[DOI: 10.61882/ibj.5043]

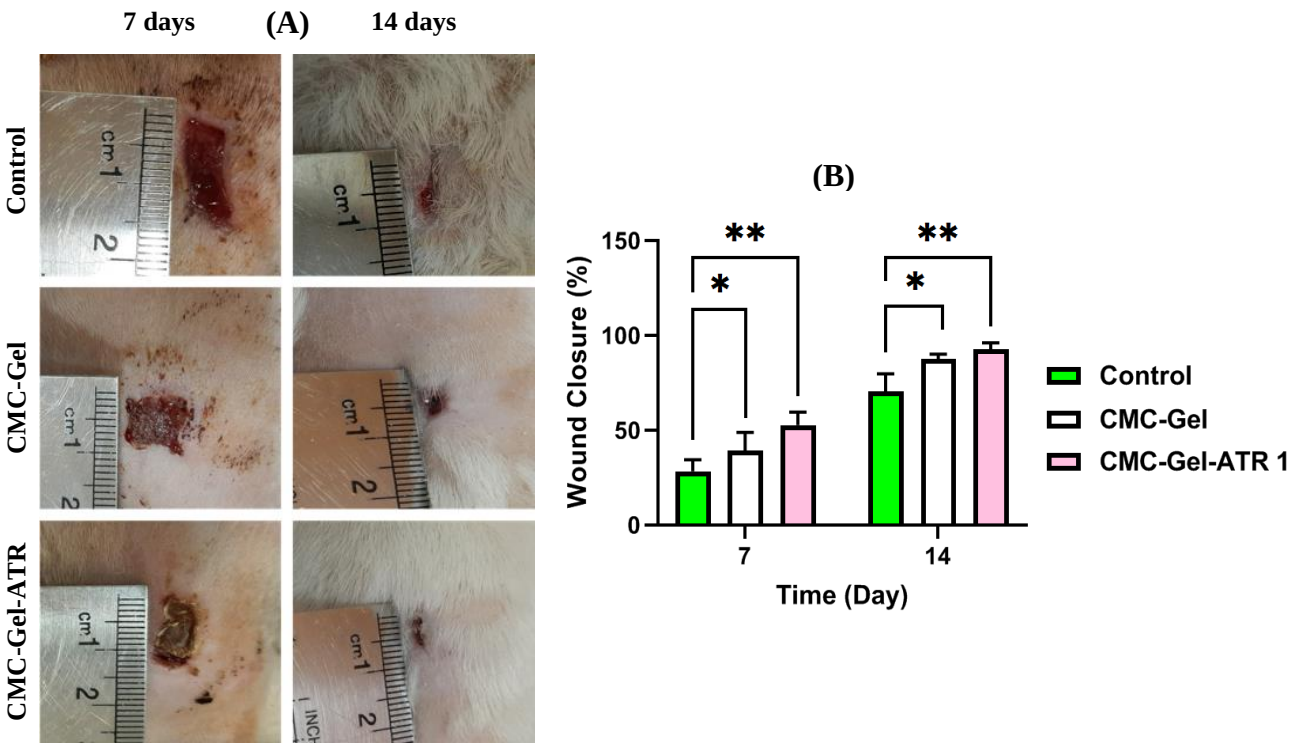

Fig 4. (A) In vivo wound-healing results; a macroscopic appearance of wounds treated with sterile gauze, CMC-Gel, and CMC-Gel-ATR1 hydrogels at 7 and 14 days post-wounding; (B) a histogram comparing the percentages of wound closure among the experimental groups after 7 and 14 days following the initial wound. Values represent the mean ± SD (n = 6); $^{*}p < 0.05$, $^{**}p < 0.01$.

Studies of the effects of ATR on the survival and function of dermal fibroblasts are very limited. In one study, the treated human dermal fibroblasts with 0.5-2.5 µM of ATR showed no toxic effects after 24 h[24]. Another study has reported that concentrations more than 20 µM at 72 h, could significantly decrease the viability due to the oxidative stress and suppression of antioxidant enzymes[25]. MTT results from our study support that lower ATR concentrations are safe, while higher concentrations showed cytotoxicity. Heit et al. have suggested that scaffold pore sizes between 20 and 120 µm are optimal for wound healing because they facilitate cell migration[26]. The optimal range of scaffold pore size suggests their potential to support efficient cell migration and nutrient exchange[25]. Gradual degradation of the scaffolds is crucial to avoid inflammation from residual materials and support cell growth. The scaffolds retained favorable biodegradability even after drug incorporation. CMC and gel scaffolds adsorb and retain moisture due to their hydrophilic and porous structure, aiding chronic wound management. Moisture retention not only prevents wound dryness but also enhances the controlled release of ATR. Likewise, scaffold swelling influences drug permeability and diffusion rate [27].

Water uptake analysis confirmed the ability of hydrogels to maintain a moist environment, which is essential for wound healing[23]. The initial interaction between the implanted wound dressing and red blood cells induces an inflammatory response. Zhou and Yi have corroborated that the acceptable hemolysis threshold for wound dressings is below 5%[14]. Blood compatibility results of our study showed that all formulations have remained below the critical 5% hemolysis threshold, except for ATR20. This finding indicates a concentration-dependent hemocompatibility, which is essential for clinical applications. Platelet aggregation and coagulation are crucial for hemostasis, i.e. a higher BCI suggests slower clotting and enhanced blood compatibility[27]. A trial involving hypercholesterolemia patients has found that 24 weeks of ATR administration reduces mean platelet volume and the neutrophil-to-lymphocyte ratio, suggesting antiplatelet and anti-inflammatory effects of ATR[28]. Thus, the use of ATR in wound dressings is concentration-dependent in which high doses can impair clotting and are unsuitable for treating bleeding wounds.

The range of pH in the wound environment plays a critical role in the healing process. The alkaline pH range (7.15–8.9), which is common in chronic wounds,

[Downloaded from ibj1.pasteur.ac.ir on 2026-10-17]

[DOI: 10.61882/ibj.5043]

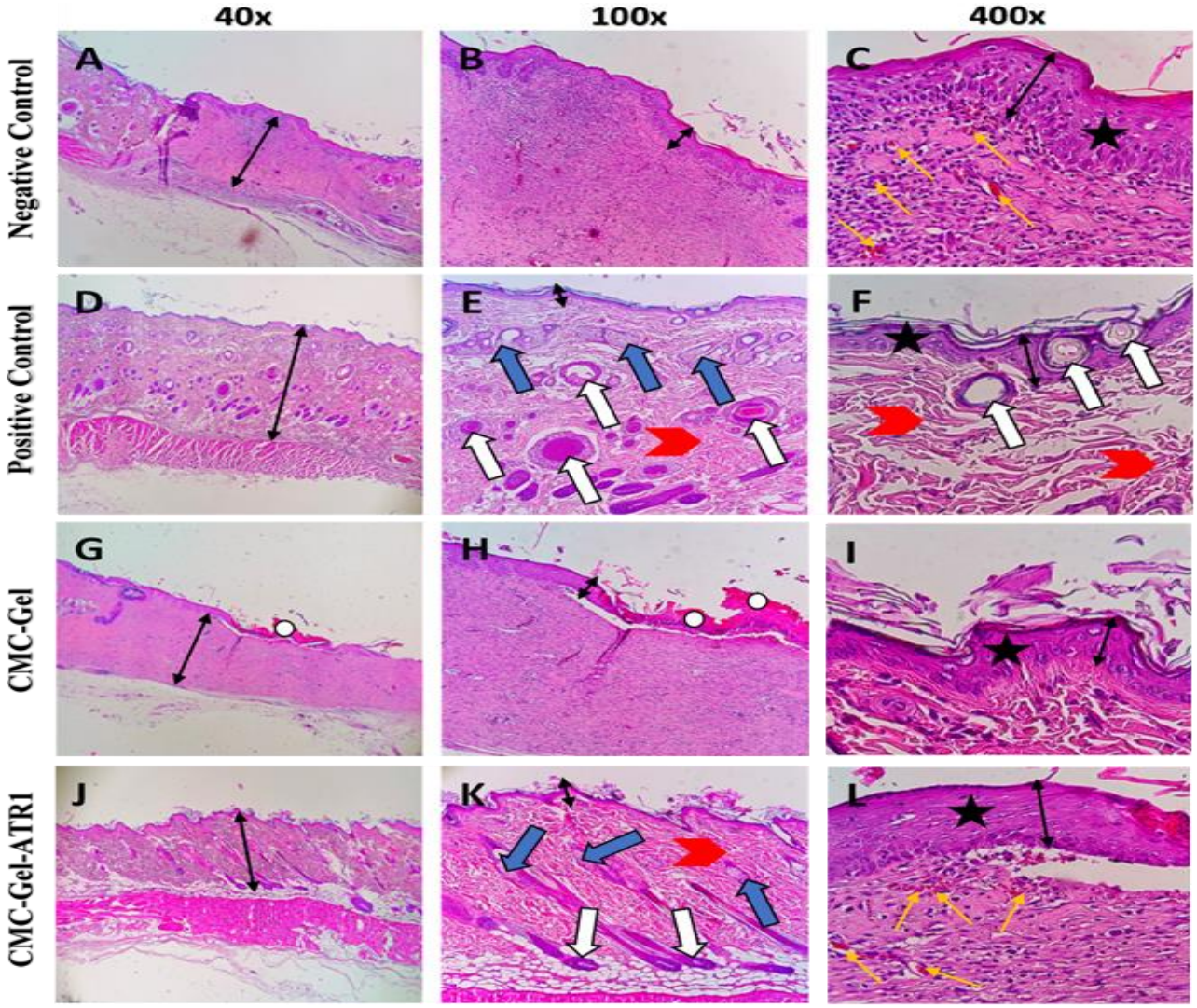

Fig 5. Microscopic sections of the healed incision wounds, stained with H & E on day 14. Negative control (A, B, C); positive control (D, E, F); CMC-Gel hydrogel (G, H, I); CMC-Gel-ATR1 hydrogel (J, K, L). Black stars: epithelialization, white arrows: hair follicle, blue arrows: sebaceous glands, red arrowheads: mature collagen, yellow arrows: neovasculation.

slows down healing, whereas an acidic environment promotes healing. Based on our results, all ATR-loaded samples showed acidic pH, which supports wound healing[29]. In vivo data corroborated our in vitro findings, showing that ATR at a concentration of 1 µM accelerates wound closure and reduces inflammation.

Histological outcomes confirmed that the CMC-Gel-ATR1 is more similar to the positive control in terms of the organized epithelialization, vascularization, appendage formation, and collagen maturity.

ATR shows considerable promise for wound healing; however, caution is warranted regarding the disadvantages and limitations noted in the research, particularly the formulation of appropriate drug concentrations. This study was limited to full-thickness cutaneous wounds and did not address chronic or complex wound types, such as burns, pressure ulcers, or diabetic wounds, which represent clinical challenges.

CONCLUSION

In this study, CMC-Gel and CMC-Gel-ATR hydrogels were successfully synthesized and evaluated as promising wound dressing compounds. We suggest CMC-Gel-ATR as a favorable wound dressing with desirable properties, making it a candidate for clinical usage.

[Downloaded from ibj1.pasteur.ac.ir on 2026-10-17]

[DOI: 10.61882/ibj.5043]

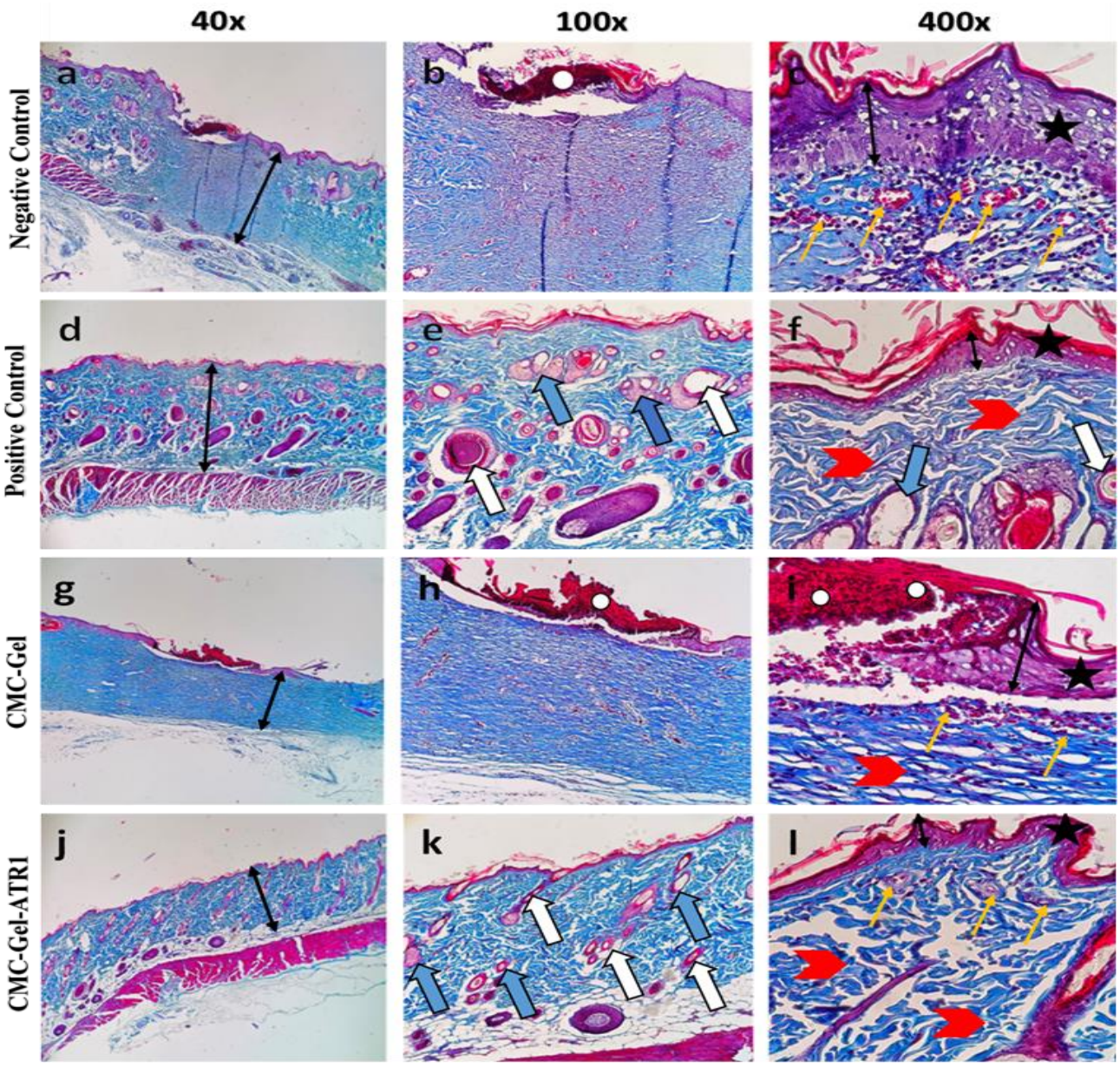

Fig 6. Microscopic sections of with the healed incision wounds stained with Masson's trichrome on day 14. Negative control (A, B, C), positive control (D, E, F); CMC-Gel hydrogel (G, H, I); CMC-Gel-ATR1 hydrogel (J, K, L). Black stars: epithelialization, white arrows: hair follicle, blue arrows: sebaceous glands, red arrowheads: mature collagen, yellow arrows: neovasculation.

DECLARATIONS

Acknowledgments

The results presented in this article are part of Seyed-Reza Mousavi's thesis. We would like to appreciate Dana Company (Tabriz, Iran) for donating the drug atorvastatin. The authors also extend their gratitude to DeepSeek, an advanced artificial intelligence platform, for its invaluable assistance in refining the language and enhancing the clarity of this manuscript. While the intellectual content and scientific contributions are the solely responsibility of the authors, we appreciate the support provided by DeepSeek in streamlining the editorial process.

Ethical approval

Animal experiments were approved by the Ethics Committee of Ahvaz Jundishapur University of Medical Sciences, Ahvaz, Iran (ethical code: IR.AJUMS.REC. 1402.513).

[Downloaded from ibj1.pasteur.ac.ir on 2026-10-17]

[DOI: 10.61882/ibj.5043]

Consent to participate

Not applicable.

Consent for publication

All authors have approved the manuscript and agree with its submission to IBJ.

Authors' contributions

SRM: performed experiments, evaluated the data, discussed the results and strategy, and prepared the article draft; MR, AK and MK: contributed in a part of the project management; MS designed and managed the study; SZ: performed experiments, evaluated the data, discussed the results and strategy, and prepared the article draft; GM: designed and managed the study.

Data availability

All relevant data can be found within the manuscript.

Competing interests

The authors declare no conflict of interest.

Funding

This work was supported by Hyperlipidemia Research Center, Ahvaz Jundishapur University of Medical Sciences, Ahvaz, Iran [grant no. HLRC-0207].

Supplementary information

The online version does not contain supplementary material.

REFERENCES

1. Griffiths CE, Barker J, Bleiker TO,Hussain W, Simpson RC, editors. Rook's textbook of dermatology, 4 Volume Set, 10th Edition. Wiley-Blackwell; 2024.
2. Farahani M, Shafiee A. Wound healing: From passive to smart dressings. Adv Healthc Mater. 2021;10(16):2100477.
3. Levine JM, Delmore B, Cox J. Skin failure: Concept review and proposed model. Adv Skin Wound Care. 2022;35(3):139-48.
4. 4. Rahman MS, Hasan MS, Nitai AS, Nam S, Karmakar AK, Ahsan MS, et al. Recent developments of carboxymethyl cellulose. Polymers. 2021;13(8):1345.
5. Kang JI, Park KM. Advances in gelatin-based hydrogels for wound management. J Mater Chem B. 2021;9(6):1503-20.
6. Feingold KR. Cholesterol lowering drugs. In: Feingold KR, Ahmed SF, Anawalt B, Blackman MR, Boyce A, Chrousos G, Corpas E, de Herder WW, Dhatariya K, Dungan K, Hofland J, Kalra S, Kaltsas G, Kapoor N, Koch C, Kopp P, Korbonits M, Kovacs CS, Kuohung W, Laferrère B, Levy M, McGee EA, McLachlan R, Muzumdar R, Purnell J, Rey R, Sahay R, Shah AS, Singer F, Sperling MA, Stratakis CA, Trence DL, Wilson DP, editors. 2024. Endotext [Internet]. South Dartmouth (MA): MDText.com, Inc.; 2000–. PMID: 27809434
7. Zahedipour F, Hosseini SA, Reiner Z, Tedeschi-Reiner E, Jamialahmadi T, Sahebkar A. Therapeutic effects of statins: Promising drug for topical and transdermal administration. Curr Med Chem. 2024;31(21):3149-66.
8. Saghafi F, Ramezani V, Jafari-Nedooshan J, Zarekamali J, Kargar S, Tabatabaei SM, et al. Efficacy of topical atorvastatin-loaded emulgel and nano-emulgel 1% on post-laparotomy pain and wound healing: A randomized double-blind placebo-controlled clinical trial. Int Wound J. 2023;20(10):4006-14.
9. Zamani S, Salehi M, Abbaszadeh-Goudarzi G, Cheraghali D, Ehterami A, Esmaili S, et al. Evaluation effect of alginate hydrogel containing losartan on wound healing and gene expression. J Biomater Appl. 2025;39(7):762-88.
10. Hoque J, Prakash RG, Paramanandham K, Shome BR, Haldar J. Biocompatible injectable hydrogel with potent wound healing and antibacterial properties. Mol Pharm. 2017;14(4):1218-30.
11. Karvinen J, Kellomäki M. Characterization of self-healing hydrogels for biomedical applications. Eur Polym J. 2022;181:111641.
12. Xu Y, Chen H, Fang Y, Wu J. Hydrogel combined with phototherapy in wound healing. Adv Healthc Mater. 2022;11(16):2200494.
13. Sideek SA, El-Nassan HB, Fares AR, Elkasabgy NA, ElMeshad AN. Cross-linked alginate dialdehyde/chitosan hydrogel encompassing curcumin-loaded bilosomes for enhanced wound healing activity. Pharmaceutics. 2024;16(1):90.
14. Zhou C, Yi Z. Blood-compatibility of polyurethane/liquid crystal composite membranes. Biomaterials. 1999;20(22):2093-9.
15. Dawit H, Zhao Y, Wang J, Pei R. Advances in conductive hydrogels for neural recording and stimulation. Biomater Sci. 2024;12(11):2786-800.
16. Buranaamnuay K. The MTT assay application to measure the viability of spermatozoa: A variety of the assay protocols. Open Vet J. 2021;11(2):251-69.
17. Hamache T, Belboukhari N, Sekkoum K. Stereochemical of atorvastatin drug by using spectroscopic. Analysis. Clinical Trials and Case Studies. 2024;3(1):1-4.
18. Tavakoli J, Tang Y. Hydrogel based sensors for biomedical applications: An updated review. Polymers. 2017;9(8):364.
19. Salehi M, Ehterami A, Farzamfar S, Vaez A, Ebrahimi-Barough S. Accelerating healing of excisional wound with alginate hydrogel containing naringenin in rat model. Drug Deliv Transl Res. 2021;11:142-53.
20. Arabpour Z, Abedi F, Salehi M, Baharnoori SM, Soleimani M, Djalilian AR. Hydrogel-based skin regeneration. Int J Mol Sci. 2024;25(4):1982.
21. Zhang Z, Feng Y, Wang L, Liu D, Qin C, Shi Y. A review of preparation methods of porous skin tissue engineering scaffolds. Mater Today commun. 2022;32:104109.
22. Liang Y, He J, Guo B. Functional hydrogels as wound dressing to enhance wound healing. ACS Nano. 2021;15(8):12687-722.

[Downloaded from ibj1.pasteur.ac.ir on 2026-10-17]

[DOI: 10.61882/ibj.5043]

23. Soleimani Z, Baharifar H, Najmoddin N, Khoshnevisan K. Evaluation of carboxymethyl cellulose/gelatin hydrogel-based dressing containing cefdinir for wound healing promotion in animal model. Gels. 2025;11(1):38.
24. Abootorabi S, Akbari J, Saeedi M, Seyedabadi M, Ranaee M, Asare-Addo K, et al. Atorvastatin entrapped noisome (Atrosome): Green preparation approach for wound healing. AAPS Pharm Sci Tech. 2022;23(3): Article number 1.
25. Marcheggiani F, Cirilli I, Orlando P, Silvestri S, Vogelsang A, Knott A, et al. Modulation of Coenzyme Q_{10} content and oxidative status in human dermal fibroblasts using HMG-CoA reductase inhibitor over a broad range of concentrations. From mitohormesis to mitochondrial dysfunction and accelerated aging. Aging. 2019;11(9):2565-82.
26. Heit YI, Dastouri P, Helm DL, Pietramaggiori G, Younan G, Erba P, et al. Foam pore size is a critical interface parameter of suction-based wound healing devices. Plast Reconstr Surg. 2012;129(3):589-97.
27. Montazerian H, Davoodi E, Baidya A, Baghdasarian S, Sarikhani E, Meyer CE, et al. Engineered hemostatic biomaterials for sealing wounds. Chem Rev. 2022;122(15):12864-903.
28. Akin F, Ayca B, Kose N, Sahin I, Akin MN, Canbek TD, et bal. Effect of atorvastatin on hematologic parameters in patients with hypercholesterolemia. Angiology. 2013;64(8):621-5.
29. Proksch E. pH in nature, humans and skin. J Dermatol. 2018;45(9):1044-52.

[Downloaded from ibj1.pasteur.ac.ir on 2026-10-17]

[DOI: 10.61882/ibj.5043]